Hydrology and Earth System Sciences
Open Access
Discussions

Testing the realism of a topography driven model (FLEX-Topo) in the nested catchments of the Upper Heihe, China

H. Gao[1], M. Hrachowitz[1], F. Fenicia[2,1], S. Gharari[1,2], and H. H. G. Savenije[1]

[1]Department of Water Management, Faculty of Civil Engineering and Geosciences, Delft University of Technology, Stevinweg 1, P.O. Box 5048, 2600 GA Delft, the Netherlands
[2]Department of Environment and Agro-Biotechnologies, Centre de Recherche Public-Gabriel Lippmann, Belvaux, Luxembourg

Correspondence to: H. Gao (h.gao-1@tudelft.nl) and M. Hrachowitz (m.hrachowitz@tudelft.nl)

Discussion Paper | Discussion Paper | Discussion Paper | Discussion Paper

HESSD

10, 12663–12716, 2013

Realism test of FLEX-Topo in the Upper Heihe

H. Gao et al.

Title Page

Abstract | Introduction

Conclusions | References

Tables | Figures

◄◄ | ►►

◄ | ►

Back | Close

Full Screen / Esc

Printer-friendly Version

Interactive Discussion

Abstract

Although elevation data is globally available, and used in many existing hydrological models, its information content is still poorly understood and under-exploited. Topography is closely related to geology, soil, climate and land cover. As a result, it may reflect the dominant hydrological processes in a catchment. In this study, we evaluated this hypothesis through three progressively more complex conceptual rainfall-runoff models. The first model ($FLEX^L$) is lumped, and it does not make use of elevation data. The second model ($FLEX^D$) is semi-distributed. It also does not make use of elevation data, but it accounts for input spatial variability. The third model ($FLEX^T$), also semi-distributed, makes explicit use of topography information. The structure of $FLEX^T$ consists of four parallel components representing the distinct hydrological function of different landscape elements. These elements were determined based on a topography based landscape classification approach. All models were calibrated and validated at the catchment outlet. Additionally, the models were evaluated at two nested sub-catchments. $FLEX^T$, performs better than the other models in the nested sub-catchment validation and it is therefore better transferable. This supports the following hypotheses: (1) topography can be used as an integrated indicator to distinguish landscape elements with different hydrological function; (2) the model structure of $FLEX^T$ is much better equipped to represent hydrological signatures than a lumped or semi-distributed model, and hence has a more realistic model structure and parameterization; (3) the wetland/terrace and grassland hillslope landscape elements of the Upper Heihe contribute the main part of the fast runoff while the bare soil/rock landscape provides the main contribution to the groundwater. Most of the precipitation on the forested hillslopes is evaporated, thus generating relatively little runoff.

1 Introduction

Topography plays an important role in hydrological processes at the catchment scale (Savenije, 2010). Topography may not only be a good first-order indicator of how water is routed through and released from a catchment (Knudsen et al., 1986), but it also has considerable influence on the dominant hydrological processes in different parts of a catchment, which could be used to define hydrologically different response units (Savenije, 2010). Thirdly, as a main indicator for hydrological behavior, topography is also closely correlated with geology, soil characteristics, land cover and climate (Savenije, 2010; Dooge, 2005; Sivapalan, 2009). Thus, information on other features can to some extent be inferred from topography. However, the information provided by topography is generally under-exploited when it comes to hydrological models although it is, explicitly or implicitly, incorporated in many models (e.g. Beven and Kirkby, 1979; Knudsen et al., 1986; Uhlenbrook et al., 2004).

As a typical lumped topography driven model, TOPMODEL (Beven and Kirkby, 1979) uses the Topographic Wetness Index (TWI) (Beven and Kirkby, 1979), which is a proxy for the probability of saturation of each point in a catchment, to consider the influence of topography on the occurrence of Saturated Overland Flow (SOF). Similarly, the Xinanjiang model (Zhao, 1992) implicitly considers the influence of topography in its soil moisture function. The curve of the tension water capacity distribution implicitly considers the influence of topographic heterogeneity. Conceptually, both models are based on the variable contributing area (VCA) concept. Although the topography-aided VCA representation is present in many models, experimental evidence has shown that it is not always realistic (Western et al., 1999; Spence and Woo, 2003; Tromp-van Meerveld and McDonnell, 2006). In view of the above discrepancies of TOPMODEL type models and in spite of its suitability in the glaciated topography of peat-dominated British-uplands and similar regions, there is an urgent need to explore new and potentially more generally applicable ways to incorporate topographic information in conceptual hydrological models.

Another type of topographically driven hydrological models are distributed physical-based models, which use topography essentially to define flow gradients and flow paths of water (Refsgaard and Knudsen, 1996). But they fail to extract additional information from topography, by which dominant runoff generating mechanisms can be identified. Further limitations of this kind of reductionist model approaches include the increased computational cost, and maybe more importantly the unaccounted scale effects (Abbott and Refsgaard, 1996; Beven and Germann, 2013; Hrachowitz et al., 2013b). Knudsen et al. (1986) developed a semi-distributed physically based model, which divides the whole catchment into several distinct hydrological response units defined by the catchment characteristics such as meteorological conditions, topography, vegetation and soil types. Although this kind of model was shown to work well in case studies, approaches like this are not widely used in application due to their intensive data requirement and complex model structure, similar to modeling approaches based on the Dominant Runoff Process concept (Grayson and Blöschl, 2001; Scherrer and Naef, 2003). In light of the above limitations, and with the purpose to conceptualize the catchment runoff yield in more realistic ways, it is important to investigate a more efficient use of topographic data and better understand their information content.

The recently suggested topography driven conceptual modeling approach (FLEX-Topo) (Savenije, 2010), which attempts to exploit topographic signatures to design conceptual model structures as a means to find the simplest way to represent the complexity and heterogeneity of hydrological processes, is the middle way between parsimonious lumped and complex distributed models (Savenije, 2010). In the framework of FLEX-Topo, topographic information is regarded as the main indicator of landscape classes and dominant hydrological processes. A valuable key for hydrologically meaningful landscape classification is, the recently introduced metric HAND (Height Above the Nearest Drainage) (Rennó et al., 2008; Nobre et al., 2011; Gharari et al., 2011), which is a direct reflection of hydraulic head to the nearest drain (Gharari et al., 2011) and can be used together with local slope. Consequently, within a flexible modelling framework (Fenicia et al., 2008, 2011), different model structures can be developed to

represent the different dominant hydrological processes in different landscape classes. Note that FLEX-Topo is not another conceptual model but rather a modeling framework to make more exhaustive use of topographical information in hydrological models and it can in principal be applied to any type of conceptual model class.

Model transferability is one of the important indicators to test model realism (Kle-meš, 1986). Although many hydrological models, both lumped and distributed, frequently perform well in calibration, transferring them and their parameter sets into other catchments or even only into sub-catchments remains problematic (Pokhrel and Gupta, 2011). There are several reasons for this: uncertainty in the data, insufficient information provided by the hydrograph or an unsuitable model structure which does not sufficiently well represent the dominant hydrological processes and/or their spatial heterogeneity (Gupta et al., 2008). Various techniques to improve model transferability were suggested in the past (Seibert and McDonnell, 2002; Uhlenbrook and Leibundgut, 2002; Khu et al., 2008; Gharari et al., 2013b; Euser et al., 2013; Hrachowitz et al., 2013b), and it became clear that successful transferability critically depends on appropriate methods to link catchment characteristics to model structures and parameters or in other words to link catchment form to hydrological function (Gupta et al., 2008).

In this study, the recently proposed topography driven modeling approach (FLEX-Topo) (Savenije, 2010) is applied and tested by a tailor-made hydrological model for a cold large river basin in Northwest China. A lumped conceptual model with lumped input data (FLEX^L) and a lumped model with semi-distributed input data (FLEX^D) are used as benchmarks to assess the additional value of the topography driven semi-distributed modeling approach (FLEX^T). The models are used as tools for testing different hypotheses within a flexible modeling framework (Fenicia et al., 2008, 2011). The objectives of this study are thus to (1) develop a topography driven semi-distributed conceptual hydrological model (FLEX^T), based on topography driven landscape classification and compare it to lumped model set-ups with varying degrees of input heterogeneity (FLEX^L, FLEX^D), (2) assess the differences in transferability of the three

models, to two uncalibrated nested sub-catchments in the study basin, thereby testing their predictive power and realism.

2 Study site

The Upper Heihe River Basin (hereafter referred to as Upper Heihe) is part of the second largest inland river in China which, from its source in the Qilian Mountains, drains into two lakes in the Gobi desert. The Upper Heihe is located in the south-west of Qilian Mountain in northwestern China (Fig. 1a). It is controlled by the gauging station at Yingluoxia, with a catchment area of 10 000 km^2. Two sub-catchments are gauged by Zhamashike and Qilian separately (Fig. 1b). The elevation of the Upper Heihe ranges from 1700 to 4900 m (Fig. 1b). The mountainous headwaters, which are the main runoff producing region and relatively undisturbed by human activities, are characterized by a cold desert climate. Long term average annual precipitation and potential evaporation are about 430 and 520 mm a^{-1}. Over 80 % of the annual precipitation falls from May to September. Snow normally occurs in winter but with a limited snow depth, averaging between 4 and 7 mm a^{-1} snow water equivalent (Wang et al., 2010). The Thiessen polygons of four meteorological stations in and around the Upper Heihe are shown in Fig. 1c. The soil types are mostly mountain straw and grassland soil, cold desert, chernozemic soil and chestnut colored soil. Land cover in the Upper Heihe is composed of forest (20 %), grassland (52 %), bare rock or bare soil (19 %), wetland (8 %), as well as ice and permanent snow (0.8 %) (Fig. 1d). The Upper Heihe has been subject of intensive research since the 1980s (Li et al., 2009). A number of hydrological models have been previously applied in this cold mountainous watershed (Xia et al., 2003; Li et al., 2011; Chen et al., 2003; Jia et al., 2009; Kang et al., 2002; Zhou et al., 2008; Zang et al., 2012). Because of limited water resources and the increasing water demand of industry and agriculture, the conflict between human demand and ecological demand in the lowland parts of the Heihe River becomes more and more severe. As the main

runoff producing region for the Heihe River, the Upper Heihe is thus essential for the water management of the whole river system.

The landscapes and the perceptual model of the Upper Heihe

Figure 2 illustrates different characteristic landscape elements in the Upper Heihe and can help us to guide the development of a perceptual model that reflects our under-standing of the dominant hydrological processes in the study basin (Beven, 2012; Tet-zlaff et al., 2013). Five dominant landscapes can be identified: bare rock mountain peaks, forested hillslope, grassland hillslope, terrace, and wetland. Typically, above a certain elevation, the landscape is covered by bare soil/rock (Fig. 2a), or permanent ice/snow. North-facing hillslopes tend to be covered by forest (Fig. 2b). The bottom of hillslopes and south-facing hillslopes are, in contrast, dominantly covered by grass (Fig. 2c). Terraces, which are irregularly flooded in wet periods and have comparably low terrain slopes, are mostly located between channels and hillslopes and are usually covered by grassland (Fig. 2d). Wetlands are covered by meadows and open water, located in the bottom of the valleys (Fig. 2d).

According to the landscape images and our understanding of catchment hydrologi-cal behavior, a perceptual model of the Upper Heihe was developed. Typically on bare soil/rock interception can be considered negligible due to the absence of significant vegetation cover. The bare soil/rock landscape at high elevations is further character-ized by a thin soil layer, underlain by partly weathered bedrock, with higher permeable debris slopes at lower elevations. On the rock and the thin soil, the dominant lateral runoff processes are Hortonian Overland Flow (HOF) and Saturated Overland Flow (SOF). Part of the localized overland flow may re-infiltrate, thereby feeding the debris slope and groundwater, while the rest of surface runoff, characterized by elevated sed-iment loads, is routed into streams. The picture of turbid water in the channel (Fig. 2e), illustrates the presence of soil erosion, which is likely to be caused by HOF and SOF in the bare soil/rock hillslopes. On the grass and forest covered hillslopes, preferen-tial flow or Subsurface Storm Flow (SSF) are the dominant hydrological processes as

Title Page

Abstract | Introduction

Conclusions | References

Tables | Figures

◄ | ►►

◄ | ►

Back | Close

Full Screen / Esc

Printer-friendly Version

Interactive Discussion

a result of the presence of efficient subsurface drainage networks created by biological and geological activity, significantly influencing the hillslope runoff yield mechanism (Beven and Germann, 2013). It can be expected that the forest-covered hillslopes are characterized by higher interception capacities and transpiration rates than the grassland hillslopes, due to the larger leaf area index (LAI) and deeper root zone. Typically, the dominant hydrological process of wetlands and terraces is SOF, due to the high groundwater levels and related limited additional storage capacity (Savenije, 2010). For the same reason, evaporative fluxes in the wetlands can be assumed to be energy rather than moisture constrained and thus close to potential rates. Further, given the limited unsaturated storage capacity, the shallow groundwater and the proximity to the channel lag times for runoff generation in wetlands, in contrast to other landscape elements, can be considered negligible on the daily time scale.

3   Data

3.1   Data set

Meteorological data were available on a daily basis from four stations in and around the Upper Heihe (1959–1978) while daily runoff data were available for the main outlet of the basin at Yingluoxia (1959–1978) and two nested sub-catchments, Qilian (1967–1978) and Zhamashike (1959–1978). The meteorological data, as the forcing data of the hydrological models, included daily precipitation and daily mean air temperature. Because only data from four meteorological stations were available, the Thiessen polygon method (Fig. 1c) was applied to spatially extrapolate precipitation and temperature. A summary of meteorological data is given in Table 1. The basic information of the three basins is listed in Table 2. Potential evaporation was estimated by the Hamon equation (Hamon, 1961), which is based on daily average temperature.

The 90 m × 90 m Digital Elevation Model (DEM) of the study site (Fig. 1b) was obtained from http://srtm.csi.cgiar.org/ and used to derive the local topographical in-

dices HAND, slope and aspect. The Normalized Difference Vegetation Index (NDVI) map (Fig. 1e) was derived from free cloud Landsat TM maps in the summer of 2002, which were obtained from International Scientific Data Service Platform (http://www.gscloud.cn/). The land cover map (Fig. 1d) was made available by the Environmental and Ecological Science Data Center for West China.

3.2 Distribution of forcing data

The elevation of the Upper Heihe ranges from 1674 to 4918 m with only 4 meteorological stations in or around the catchment, covering an area of $10\,000\,km^2$. In addition, the meteorological stations in the Upper Heihe River are all located at relatively low elevations in the valley bottoms, which are easily accessible and to maintain but potentially unrepresentative (Klemeš, 1990). Precipitation and temperature data were thus adjusted using empirical relationships.

The entire catchment was thus first discretized into four parts by the Thiessen polygon method. Each Thiessen polygon was then further stratified into seven elevation zones. Precipitation was assumed to increase linearly with elevation increase (Eq. 1) and temperature was assumed to decrease linearly with the increase of elevation (Eq. 2) according to empirical relationships for the region obtained from literature (Wang, 2009):

$$P_j = P\left(1 + \frac{C_p(h_j - h_0)}{10\,000}\right) \tag{1}$$

$$T_j = T\left(1 - \frac{C_t(h_j - h_0)}{100}\right) \tag{2}$$

where P is the stationary observed precipitation; P_j is the interpolated precipitation in elevation h_j; h_0 is the elevation of the meteorological station; C_p $(\%\,(100\,m)^{-1})$ is the precipitation lapse rate. T is the measured temperature; T_j is the distributed temper-

ature by elevation; C_t $(°C(100\,m)^{-1})$ is the environmental temperature lapse rate. The precipitation lapse rate was set to $11.5\,mm\,(100\,m\,a)^{-1}$, a value estimated with data from several meteorological stations in and around the Upper Heihe River Basin, resulting in relative lapse rates of $3.9\,\%\,(100\,m)^{-1}$ in the Tuole polygon, $2.8\,\%\,(100\,m)^{-1}$ in the Yeniugou polygon, $8.8\,\%\,(100\,m)^{-1}$ in the Zhangye polygon and $2.9\,\%\,(100\,m)^{-1}$ in the Qilian polygon (Fig. 1c). Due to a relatively stable relationship between temperature and elevation, C_t is set to a constant value of $0.6\,°C\,(100\,m)^{-1}$. The potential evaporation is estimated in each elevation zones by the corrected temperature.

4   Modeling approach

In this study three conceptual models of different complexity were designed and tested: a lumped model (FLEX[L]), a model with semi-distributed forcing data and reservoirs but identical model structures and parameters for each of the components (FLEX[D]), and a topography driven semi-distributed model (FLEX[T]). All models are a combination of reservoirs, lag functions and connection elements connected in various ways to represent different hydrological function in the spirit of flexible modeling frameworks such as SUPERFLEX (Fenicia et al., 2011).

4.1   Lumped model (FLEX[L])

The lumped model (FLEX[L]) (Fig. 3) has a structure that is similar to that used in earlier applications of the FLEX model (Fenicia et al., 2008), and it comprises five reservoirs: a snow reservoir, an interception reservoir, an unsaturated reservoir, a fast response reservoir and a slow response reservoir. A lag function represents the lag time between storm and flood peak. The model has 12 free calibration parameters. The Thiessen polygon averaged precipitation, temperature and potential evaporation are used as forcing data.

4.1.1 Snow and interception routine

Precipitation can be stored in snow- or interception reservoirs before the water enters the unsaturated reservoir. Normally, the snow routine plays an important role in winter and spring while interception becomes more important in summer and autumn. Here it is assumed that interception happens during rainfall events when the daily air temperature is above the threshold temperature (T_t), and there is no snow cover, i.e. typically in summer. When the average daily temperature is below T_t, precipitation is stored as snow cover, which normally occurs in winter. When there is snow cover and the temperature is above T_t, P_e is equal to the sum of rainfall (P) and snowmelt (M), conditions normally prevailing in early spring and early autumn. Note that snowmelt water is conceptualized to directly infiltrate into the soil, thus effectively bypassing the interception store. In other words, interception and snowmelt never happen simultaneously. Their respective activation is controlled by air temperature, precipitation, and the presence of snow cover.

The snow routine was designed as a simple degree-day model as successfully applied in many conceptual models (Eq. 3; Gao et al., 2011; Seibert, 1997; Uhlenbrook et al., 2004; Kavetski and Kuczera, 2007; Hrachowitz et al., 2013a).

$$M = \begin{cases} \min\left(\frac{S_w}{\Delta t}, F_{DD}(T - T_t)\right) & \text{if } T > T_t \\ 0 & \text{if } T \leq T_t \end{cases} \tag{3}$$

where M (mm d^{-1}) is the snowmelt, S_w (mm) is the storage of snow reservoir, t (d) is the discretized time step, F_{DD} (mm (d °C)$^{-1}$) is the degree day factor, which defines the melted water per day per Celsius degree above T_t (°C). The interception evaporation E_i (mm d^{-1}), which cannot be larger than potential evaporation (E_p (mm d^{-1})), is calculated by an interception reservoir (S_i (mm)), with daily maximum storage capacity (I_{max} (mm d^{-1})) (Eq. 4).

Title Page

Abstract | Introduction

Conclusions | References

Tables | Figures

◄ | ►

◄ | ►

Back | Close

Full Screen / Esc

Printer-friendly Version

Interactive Discussion

$$E_i = \min\left(E_p, I_{max}, \frac{S_i}{\Delta t}\right) \tag{4}$$

4.1.2 Soil routine

The soil routine, which is the core of hydrological models, determines the amount of runoff generation. In this study, we applied the widely used Beta function of the Xinanjiang model (Eq. 5) (Zhao, 1992) to compute the runoff coefficient for each time step as a function of the relative soil moisture:

$$C_R = 1 - \left(1 - \frac{S_U}{S_{Umax}}\right)^\beta \tag{5}$$

$$R_f = C_R P_e D \tag{6}$$

$$R_s = C_R P_e (1 - D) \tag{7}$$

where C_R (–) indicates the runoff coefficient, S_U (mm) is the soil moisture content, S_{Umax} (mm) is the maximum soil moisture capacity in the root zone, and β (–) is the parameter describing the spatial process heterogeneity in the study catchment. In Eq. (6), P_e (mm d^{-1}) indicates the effective rainfall and snowmelt into soil routine; R_f represents the flow into the fast response routine; D is a splitter to separate recharge from preferential flow. In Eq. (7), R_s indicates the flow into the groundwater reservoir. S_U, S_{Umax} and potential evaporation (E_p (mm d^{-1})) were used to determine actual evaporation E_a (mm d^{-1}; Eq. 8).

$$E_a = E_p \min\left(\frac{S_U}{S_{Umax} C_e}, 1\right) \tag{8}$$

where C_e (–) is the fraction of S_{Umax} above which the actual evaporation is equal to potential evaporation, here taken as 0.5 (Savenije, 1997); otherwise E_a is constrained by the water available in S_U.

4.1.3 Response routine

A simple delay function (Eqs. 9 and 10) was used to describe the lag time between storm and peak flow:

$$R_{\mathrm{fl}}(t) = \sum_{i=1}^{T_{\mathrm{lag}}} c(i)\, R_{\mathrm{f}}(t - i + 1) \tag{9}$$

where

$$c(i) = \frac{i}{\sum_{u=1}^{T_{\mathrm{lag}}} u} \tag{10}$$

where $R_{\mathrm{f}}(t - i + 1)$ is the generated fast runoff in the unsaturated zone at time $t - i + 1$, T_{lag} is a parameter which represents the time lag between storm and fast runoff generation, $c(i)$ is the weight of the flow in $i - 1$ days before and $R_{\mathrm{fl}}(t)$ is the discharge into the fast response reservoir after the convolution by the Eq. (10). The linear response reservoirs, representing a linear relationship between storage and release, are applied to conceptualize the discharge from the surface runoff reservoir (Eq. 11), fast response reservoirs (Eq. 12) and slow response reservoirs (Eq. 13).

$$Q_{\mathrm{ff}} = \frac{\max(0,\, S_{\mathrm{f}} - S_{\mathrm{fmax}})}{K_{\mathrm{ff}}} \tag{11}$$

$$Q_{\mathrm{f}} = \frac{S_{\mathrm{f}}}{K_{\mathrm{f}}} \tag{12}$$

$$Q_{\mathrm{s}} = \frac{S_{\mathrm{s}}}{K_{\mathrm{s}}} \tag{13}$$

$$Q = Q_{\mathrm{ff}} + Q_{\mathrm{f}} + Q_{\mathrm{s}} \tag{14}$$

where Q_{ff} (mm d^{-1}) is the surface runoff, with timescale K_{ff} (d), active when the storage of fast response reservoir exceeds the threshold S_{fmax} (mm). Q_f (mm d^{-1}) and Q_s (mm d^{-1}) represent the fast and slow runoff; S_f (mm) and S_s (mm) represent the storage state of the fast and the groundwater reservoirs; K_f (d) and K_s (d) are the time scales of the fast and slow runoff, respectively, while Q (mm d^{-1}) is the total modeled runoff from the three individual components (Eq. 14).

4.2 Lumped model with semi-distributed forcing data (FLEX^D)

In order to test the influence of distributing the input forcing data and moisture accounting, a semi-distributed model (FLEX^D) based on FLEX^L was tested. The model structure of FLEX^D is identical to FLEX^L, but it is forced with semi-distributed data (see Sect. 3.2), resulting in distributed moisture accounting between the individual parallel model structures, representing the influence areas of the 4 Thiessen polygons and the 7 elevation bands in the study area (Fig. 4). Note that the groundwater reservoir is treated as lumped and that except for the lag times all parameters are identical for the 28 parallel modeling units. As shown in Table 4, the T_{lagT} T_{lagY} and T_{lagQ} represent the lag time from the Tuole, Yeniugou, and Qilian Thiessen polygons to the Yingluoxia outlet respectively. The time lag of Zhangye polygon is negligible, due to the polygons proximity to the outlet.

4.3 Topography driven, semi-distributed model (FLEX^T)

According to the perceptual model of the Upper Heihe (see Sect. 2.1), the hypotheses that different observable landscape units are associated with different dominant hydrological processes was tested by incorporating these units into hydrological models.

4.3.1 Landscape classification

In this study, Height Above the Nearest Drainage (HAND) (Rennó et al., 2008; Nobre et al., 2011; Gharari et al., 2011), elevation, slope and aspect (Fig. 5) were used for deriving a hydrologically meaningful landscape classification. The stream initiation threshold for estimating HAND was set to 20 cells ($0.16\,km^2$), which was selected to maintain a close correspondence between the derived stream network and that of the topographical map. The HAND threshold value for distinction between wetland and other landscapes was set at 5 m, similar to what was used in earlier studies (Gharari et al., 2011). If HAND is larger than 5 m, but the local slope is less than 0.1, the landscape element is defined as terrace. The most dominant landscape in the Upper Heihe, however, is the hillslope, which has been further separated into three sub-classes according to HAND, absolute elevation, aspect and vegetation cover (Fig. 5). Thus, hillslopes above 3800 m and with HAND > 80 m, typically characterized by bare soil/rock have been according defined as bare soil/rock hillslopes. At elevations between 3200 and 3600 m and aspect between 225 and 135°, or at elevations below 3200 m and aspect between 270 and 90°, hillslopes in the Upper Heihe are generally forested (Jin et al., 2008) and thus have been defined as forest hillslopes. The remaining hillslopes were defined as grassland hillslopes. From the classification map (Fig. 6b), it can be seen that the landscape classification is similar to the independently obtained land cover map (Fig. 6a), except for the area of wetland, due to different definitions between the land cover map and our classification. Note that wetland and terrace landscape classes have been combined (Fig. 6c), because the area proportion of wetlands varies over time, while terraces may be flooded at times, which can be described by the VCA concept. This combination is unlikely to reduce realism and makes the model simpler. Consequently, the NDVI map has been averaged in accordance with this classification (Fig. 6c).

4.3.2 FLEX^T model structure

Based on the landscape classification and the perceptual models for each landscape, different model structures to represent the different dominant hydrological processes were then assigned to the four individual landscape classes (Table 3). The four model structures are running in parallel, except for the groundwater reservoir (Fig. 7). The snowmelt process is considered in all landscapes by the same method as described in Sect. 4.1.1. In the bare soil/rock class, the HOF (R_{HB} ($mm\,d^{-1}$)) is controlled by a threshold value (P_t ($mm\,d^{-1}$)) (Eq. 15). HOF only occurs when the daily effective precipitation (P_{eB}) is larger than P_t:

$$R_{HB} = \max(P_{eB} - P_t, 0). \tag{15}$$

SOF (R_{SB} ($mm\,d^{-1}$)) happens when the amount of water in the unsaturated reservoir exceeds the storage capacity ($S_{UB} > S_{UmaxB}$). Deep percolation from bare soil/rock into groundwater (R_{pB} ($mm\,d^{-1}$)) is controlled by the relative soil moisture (S_{UB}/S_{UmaxB}) and maximum percolation (P_{ercB} ($mm\,d^{-1}$)):

$$R_{pB} = P_{ercB} \frac{S_{UB}}{S_{Umax}}. \tag{16}$$

The actual evaporation (E_{aB}) is estimated by the relationship between relative soil moisture and potential evaporation (E_{pB}), the same as Eq. (16). The generated surface runoff on the bare soil/rock is separated into water re-infiltrating (R_{rB}) while flowing on the higher permeable debris slopes and the water directly routed to the channel (R_{ffB}) by a separator (D_B). As in FLEX^D, the lag times are characterized by different lengths in the individual components. The response process of the surface runoff is controlled by a linear reservoir, as Eq. (12).

The grassland and forest hillslopes have the same model structure as FLEX^L, due to their similar runoff producing mechanisms, but are characterized by different parameter values for interception (I_{maxGH} ($mm\,d^{-1}$) and I_{maxFH} ($mm\,d^{-1}$)), and unsaturated zone

processes (S_{UmaxGH} (mm), S_{UmaxFH} (mm) and β_{GH} (–) β_{FH} (–)), reflecting different land cover, and root zone depth. The lag times of grassland and forest hillslopes are the same as in the bare soil/rock landcape elements. In wetland/terrace, additionally capillary rise is represented by a parameter (C_{r} ($\mathrm{mm\,d^{-1}}$)) indicating a constant amount
5 of capillary rise. The calculation method of effective rainfall and actual transpiration is the same as grassland and forest hillslopes. The lag time of storm-runoff in wetland is neglected. The groundwater was assumed to be generated from one single aquifer in the catchment, and represented by a lumped linear reservoir, as Eq. (13). The final simulated runoff is equal to the sum of runoffs from all landscape elements according
10 to their proportions (Fig. 7).

4.4 Model calibration

4.4.1 Objective functions

To allow for the model to adequately reproduce different aspects of the hydrological response, i.e. high flow, low flow and the flow duration curve, and thereby increase
15 model realism, a multi-objective calibration strategy was adopted in this study, using the Nash-Sutcliffe efficiency (NSE) (Nash and Sutcliffe, 1970) of the hydrographs (I_{NS}) to evaluate the model performance during high flow, the NSE of the flow duration curve (I_{NSF}) to evaluate the simulated flow frequency and the NSE of the logarithmic flow (I_{NSL}) which emphasizes the lower part of the hydrograph. The I_{NS}, is mostly an indi-
20 cator of model fit to the high flow; the I_{NSF} indicates the fit to the flow duration curve; similarly, the I_{NSL} is an indicator of the fit to the low flow.

4.4.2 Calibration method

The groundwater recession parameter (K_{s}) not treated as free parameter but it is rather obtained directly from the observed hydrograph using a Master Recession Curve ap-

Title Page

Abstract | Introduction

Conclusions | References

Tables | Figures

◄ | ►►

◄ | ►

Back | Close

Full Screen / Esc

Printer-friendly Version

Interactive Discussion

proach (MRC) (Lamb and Beven, 1997; Fenicia et al., 2006). Therefore K_s was fixed at 90 (d) to avoid its interference on other processes.

The MOSCEM-UA (Multi Objective Shuffled Complex Evolution-University of Arizona) algorithm (Vrugt et al., 2003) was used as the calibration algorithm to find the Pareto-optimal fronts of the three objective functions. There are three parameters to be set for MOSECEM-UA: the maximum number of iterations, the number of complexes, and the number of random samples that is used to initialize each complex. For the FLEX^L model the number of iterations was set to 50 000, the number of complexes to 10 and the number of random samples to 1000. To account for increase model complexity, the parameters of the FLEX^D were set as 50 000, 12 and 1440; the parameters of the FLEX^T are set as 50 000, 22 and 4840. The uniform prior parameter distributions of FLEX^L and FLEX^D are listed in Table 4 and the ones of FLEX^T are given in Table 5.

4.4.3 Constraints on FLEX^T parameters and fluxes

Guided by our perceptual understanding of the study catchment in Sect. 2.1 and the NDVI map (Fig. 6c), a set of constraints for model parameters and simulated fluxes was developed. Parameter sets and model simulations that do not respect these constraints were regarded as non-behavioral parameters, and rejected during calibration. More specifically, the parameters related to interception evaporation and transpiration were constrained based on expert knowledge (Table 6). It was assumed that the interception threshold in the forest class (I_{maxFH}) needs to be larger than in the grassland (I_{maxGH}) and wetland/terrace classes (I_{maxW}), due to the increased interception capacity of forests. In addition, the root zone depth of forest hillslopes (S_{UmaxFH}) should be deeper than in grassland (S_{UmaxGH}). Furthermore, the root zone depth of wetland/terrace (S_{UmaxW}) and bare soil/rock (S_{UmaxB}) are assumed to be shallower than those of hillslopes. The time-scale of groundwater (K_s) was to be the highest due to its slow recession process, while the time scales of SOF in the wetland/terrace class (K_r) and the surface runoff in the bare soil/rock hillslope class (K_{ff}) were defined to be the shortest, with the time scale of SSF (K_f) on forest and grassland hillslope assumed

to be in-between. Further soft knowledge was used to constrain the simulated results, to avoid unreasonable trade-off among fluxes in different landscapes (Table 6). The combined evaporation and transpiration in forest ($E_{iFH} + E_{aFH}$ the unit is $mm\,a^{-1}$ hereinafter) should be larger than in grassland ($E_{iGH} + E_{aGH}$), due to the higher vegetation cover in forests (see the NDVI map in Fig. 6c). Similarly, the evaporative fluxes from wetland/terrace ($E_{iW} + E_{aW}$) are assumed to be higher than from the grassland as they are more moisture constrained in the latter. The evaporative water loss from the bare soil/rock class (E_{iB}) is the least, due to its sparse vegetation cover and lowest temperature. Furthermore, transpiration in forest (E_{aFH}) should be expected to be higher than in grassland (E_{aGH}), because more water is needed in forest to meet its growth requirement and as deeper roots allow access to a larger pool of water.

4.5 Model evaluation

Model evaluation is usually limited to calibration followed by split-sample validation (Klemeš, 1986). Frequently, split-sample validation can result in satisfactory model performance as the model is trained by data from the same location in the preceding calibration period. On the basis of successful split-sample validation, models and their parameterizations are then often considered acceptable for predicting the rainfall-runoff response at the given study site. It has in the past, however, been observed that many models with adequate split-sample performance failed to reproduce hydrographs even of its nested sub-basins (e.g. Pokhrel and Gupta, 2011). In this study, we therefore applied the calibrated models of different complexity and degrees of input data distribution together with their calibrated parameter sets to two nested catchments to test the models' transferability and thus the ability to reproduce the hydrologic response in catchments they have not explicitly been trained for. This kind of nested sub-catchment validation can, even if it is not an entirely independent validation in the sense of a proxy-basin test (Klemeš, 1986), give crucial information on the process realism and the related predictive power of a model. In this study the hydrological data at the main outfall Yingluoxia (1959–1968) were used for model calibration. Subsequently

the model was tested by a split sample test at the main outfall (1969–1978), and its two nested stations: Qilian (1967–1978) and Zhamashike (1959–1978).

4.6   Results of FLEX^L and FLEX^D

Table 7, as well as Figs. 8a and 9a illustrate that FLEX^L performed quite well in the calibration period with respect to both the hydrograph and the flow duration curve (FDC). In spite of a somewhat reduced performance, the lumped model was also able to reproduce the major features of the catchment response in the split-sample validation (Table 7, Figs. 8b and 9b). However, when tested whether the model structure and parameter sets of FLEX^L could be used in the nested sub-catchments, in other words, testing the model's potential in an uncalibrated part of the catchment as if they were ungauged basins (Sivapalan et al., 2003; Hrachowitz et al., 2013b), the performance of FLEX^L was far from satisfactory (Table 7, Figs. 8c and d, 9c and d). The validation hydrographs in two nested sub-catchments, which are in the same period as the split-sample validation, are shown in Fig. 9c and d. One interesting observation is that the large precipitation event at the end of the warm season in 1970 did not produce any peak flow in all three catchments, a characteristic that cannot be adequately reproduced by FLEX^L (Fig. 9b–d). Similarly, the sub-catchment FDCs (Fig. 8b–d) indicate that FLEX^L, while in general mimicking well the FDC of the entire catchment, poorly represents the low flow characteristics of the two sub-catchments.

In the next step the influence of distributing the forcing input on the model performance was tested using the FLEX^D model set-up (Fig. 4). It was found that although the modelled hydrograph and FDC reflect the observed response dynamics similarly well as FLEX^L (Figs. 8a and 9a), the objective functions indicate a slightly poorer calibration performance (Table 7), in spite of two additional parameters accounting for differences in channel routing lag times. In this study, the reason is potentially related to the uncertainty in the precipitation–elevation relationship and the inappropriate soil moisture distribution dictated by the Thiessen polygons. In the split-sample and Qil-

ian sub-catchment validation (Table 7, Fig. 8b and d), FLEX^D does not add value to the results of the lumped FLEX^L model. However the validation results in Zhamashike improve with FLEX^D, with increased NSE values for both, FDC and the hydrograph (Table 7), although base flow is still not reproduced well (Fig. 8c). This indicates that at least for the Zhamashike sub-catchment the distributed precipitation is more representative than catchment averaged precipitation or that the results are more sensitive to the heterogeneity of precipitation and temperature input than in the Qilian sub-catchment. Besides that, hydrograph inspection revealed that the mismatch of observed and modelled runoff, generated by the large precipitation event at the end of the warm season was not captured well by the FLEX^D either (Fig. 9b–d), although with slight improvement (see the reasons in Sect. 6.1).

4.7 Results of FLEX^T

From Table 7, it is found that the performance of the topography driven, semi-distributed FLEX^T is stable in calibration, split-sample validation and sub-basin validation, for all three objective functions (I_{NS}, I_{NSF} and I_{NSL}), but especially the I_{NSF}. In calibration the performance of FLEX^T, as indicated by the objective functions (Table 7), is slightly lower than the performance of FLEX^L, due to the constraints imposed by soft data. However, in split-sample validation and sub-catchment validation, the performance of FLEX^T is significantly better than those of FLEX^L and FLEX^D.

In Fig. 7, the modelled fluxes, which are the average values of all the results obtained by the parameters sets on the Pareto-optimal fronts, of each landscape class for the entire catchment are given. The water balances of the individual landscape units illustrate clearly the distinct dominant hydrological functions of these individual units as a priori defined by the modeller's perception of the system. Specifically, the precipitation on bare soil/rock is $481\,\mathrm{mm\,a^{-1}}$ (18 % (hereinafter) proportion of the entire catchment precipitation), $174\,\mathrm{mm\,a^{-1}}$ (6 %) of which is evaporated. $115\,\mathrm{mm\,a^{-1}}$ (4 %) is percolated into cracks and then to the groundwater. The HOF is $74\,\mathrm{mm\,a^{-1}}$ (3 %) caused

by intensive rainfall, and 112 mm a^{-1} (4 %) is generated as SOF. Part of the generated surface runoff re-infiltrates into groundwater (107 mm a^{-1} (4 %)) due to the high permeability of debris slopes at the foot of the mountains; excess water (77 mm a^{-1} (3 %)) is routed to the channel over the surface with considerable sediment load. Precipitation on the forest hillslopes reaches 431 mm a^{-1} (17 %), 125 mm a^{-1} (5 %) of which is intercepted by the canopy and/or the topsoil layer, 257 mm a^{-1} (10 %) is modelled as transpiration, while only 26 mm a^{-1} (1 %) and 15 mm a^{-1} (0.6 %), respectively contribute to fast runoff and groundwater recharge, highlighting the evaporation function of this landscape class. The precipitation on the grassland hillslopes is 431 mm a^{-1} (31 %), 58 mm a^{-1} (4 %) of which is intercepted, 205 mm a^{-1} (15 %) of which is transpired by plants, 101 mm a^{-1} (7 %) of which generates fast runoff and 63 mm a^{-1} (5 %) recharges the groundwater. For the wetland/terrace, precipitation is 410 mm a^{-1} (34 %) and besides that around 21 mm a^{-1} (1.7 %) is fed in by groundwater as capillary rise. 87 mm a^{-1} (7 %) is intercepted; 220 mm a^{-1} (19 %) is consumed by plant transpiration and 122 mm a^{-1} (10 %) contributes to the fast runoff. Finally, the groundwater discharge is 51 mm a^{-1} (12 %), which accounts for 37 % of the total runoff. In total, the modelled runoff depth is 143 mm a^{-1}, which is close to the observed runoff (141 mm a^{-1}). For the simulated total evaporation, it is interesting to find that the ratio between forest and wetland is 1.24, which is close to their NDVI ratio (1.27). Similarly, the ratio between water loss to atmosphere in wetland and grassland is 1.21, which is also close to their NDVI ratio (1.20).

Figure 8 shows the significant improvement of FDC simulation by FLEX^T other than previous models, which indicates its capacity of better reproducing flow frequency, that is more convincing than exact hydrograph simulation (Westerberg et al., 2011). The better performance of FDC simulation by FLEX^T means that the flexibility for incorporating changing proportions of landscape elements for different catchments and constrained parameters calibration strategy in FLEX^T has the potential to substantially increase the predictive power for flow characteristics especially the low flows (Fig. 8, Table 7).

Full Screen / Esc

Printer-friendly Version

Interactive Discussion

Figure 9 shows the envelopes of observed and simulated hydrographs (based on all the parameters sets on the Pareto-optimal front) of three model structures, in calibration, validation and sub-catchments validation. The precipitation and the temperature are also shown corresponding to the time series of hydrograph. The intense-precipitation nonpeak-flow event in 1970 has been highlighted, which is well simulated by FLEX^T instead of FLEX^L or FLEX^D (see the reasons in Sect. 6.1).

The simulated hydrograph components from different landscapes are shown in Fig. 10. Generally, the hydrograph is mainly contributed by SOF from wetland/terrace, SSF from grassland hillslopes and groundwater. Specifically, the dash box in Fig. 10a shows the hydrograph components of a peak flow event. While all the landscapes contributed to the runoff, the wetland/terrace responded directly to the storm whereas the response of grassland hillslopes and bare soil/rock contributed to the peak flow later. Forest hillslopes barely contributed to this peak event. Figure 10b–d shows the hydrograph components during an intense precipitation but non-peakflow event. From the insets in this figure, it can be seen that the small peak is generated by wetland/terrace and grassland hillslopes. The bare soil/rock and forest hillslopes did not respond to this intense precipitation (see the reasons and discussion in Sect. 6.1).

5 Discussion

5.1 Why did FLEX^T perform better than FLEX^L and FLEX^D?

Some clarification can be achieved by comparing the observed precipitation duration curves (PDC) and FDC. From Fig. 11a, it can be concluded that the entire Upper Heihe receives the lowest catchment average precipitation input both in the original forcing data and the elevation corrected precipitation, while being characterized by the largest runoff yield (Fig. 11b). The Qilian sub-catchment, in contrast, receives the largest amount of precipitation, but with lower runoff yield. The Zhamashike sub-catchment is characterized by similar precipitation input as the entire Upper Heihe, but exhibits

much higher peak flows and lower base flows than both the entire catchment and the Qilian sub-catchment. These distinct catchment hydrological functions are difficult to be reconciled in one lumped model, representing a specific rainfall–runoff relationship. Moving to a different catchment or maybe only even to a nested sub-catchment is likely to change the relative proportions of landscapes, thus leading to misrepresentation of the lumped process heterogeneity and thus reduced model performance in the new catchment. A semi-distributed approach like $FLEX^T$, in contrast to $FLEX^L$ and $FLEX^D$, offers more flexibility in adapting the model to the ensemble of processes in a more realistic way other than the one trained by adjusting it to the hydrograph, which most likely oversimplifies the catchment heterogeneity. This underlines the increased importance and benefit of more detailed, yet flexible expert-knowledge guided process representations compared to focusing on mere parameter calibration of lumped models.

The potential reason of overestimating the runoff in the Zhamashike sub-catchment for $FLEX^L$ and $FLEX^D$ (Fig. 8c) is that these two models do not adequately represent the increased importance of evaporation from wetland/terrace. Similarly, the reason of overestimating flow in the Qilian sub-catchment (Fig. 8d) is that these two models cannot accommodate the increased evaporation of forests as much of the Upper Heihe, for which the models were calibrated, is covered by grassland hillslope and bare soil/rock, characterized by lower evaporation rates than the other landscapes. On the other hand, both the $FLEX^L$ and $FLEX^D$ overestimate the baseflow (Fig. 8c and d). This can potentially be linked to neglecting capillary rise in the wetland/terrace, which influences both the baseflow and the evaporation of this landscape element. Considering capillary rise in $FLEX^T$, the groundwater feeds the unsaturated reservoir in the wetland, which not only reduces the base flow but also increases the amount of water available for transpiration and eventually evaporation. This hydrological process is especially important in the Zhamashike sub-basin, where higher peak flows and lower base flow happen simultaneously.

The results support the potential of $FLEX^T$ and its parameterization to be spatially and scale-wise more transferable than lumped model structures, such as $FLEX^L$ and

FLEX^D (see Sect. 5.2). In summary, the FLEX^T model set-up, informed by topography, divided the catchments into four topographic sub-units, to be loosely interpreted as different functional Hydrological Response Units (HRUs) and representing different dominant hydrologic process ensembles. As each catchment is likely to be characterized by different proportions of the different HRUs, this kind of modelling strategy allowed enough flexibility to capture the different functional behaviours of the three study catchments simultaneously (Table 7, Figs. 9–11). The better transferability of the FLEX^T means that it is a more realistic representation of reality than the other two models.

Specific rainfall/snowfall-runoff events

Some simulated events also illustrate the realism of our model, such as the storm-flood event in Fig. 10a and the intense-precipitation but non-peakflow event (Fig. 10b–d). It was noticed that FLEX^T could reproduce the instantaneous response of the wetlands to the storm and the delayed response of other landscapes (Fig. 10a). The bare soil/rock contributed to the peak flow by HOF and SOF, due to the intense rainfall, while the wetland/terrace and the grassland hillslopes contribute to this peak event by SOF and SSF. The observed hydrographs show a further interesting event: the largest daily precipitation of the year at the end of September 1970 only produced a comparatively small runoff peak, both in the Upper Heihe and its nested sub-catchments (Fig. 9). Both, FLEX^L and FLEX^D failed to adequately reproduce this event, and modelled a much larger peak flow. Significant precipitation measurement error can be excluded, as the same phenomenon happened not only in the entire catchment but also in other two sub-catchments. One can think of several reasons behind this behaviour. Theoretically, the lumped accounting of the snowmelt in FLEX^L could partly be the reason, because the lumped model does not consider the change of temperature and then the type of precipitation with elevation. The lumped model treats the precipitation as rainfall in the entire catchment when the average daily air temperature is above the rain/snow tem-

Title Page

Abstract | Introduction

Conclusions | References

Tables | Figures

◄◄ | ►►

◄ | ►

Back | Close

Full Screen / Esc

Printer-friendly Version

Interactive Discussion

perature threshold. However, there could be snowfall in high elevation zones, when the catchment average temperature is slightly above the threshold temperature. Likewise, there could be rainfall in lower elevation zones, when the catchment average temperature is below the threshold. The temperature record (Fig. 9) clearly shows the low average air temperature on the same day as the large precipitation event. This could partly explain the limited runoff response to this specific storm event, as the modelled results obtained from FLEX^D are somewhat closer to the observed response than the results of FLEX^L (Fig. 9b and d).

However, FLEX^D could not mimic the event in a satisfactory way and hence the failure of FLEX^D to adequately represent the event can be attributed to an over-simplified model structure. This is supported by the results of FLEX^T. From Fig. 10 it can be seen that the modelled flow generated by this storm event mostly originated from the wetlands, and a smaller proportion originated from grassland hillslopes. Contribution from forest hillslopes and bare soil/rock hillslopes is negligible. The catchment average temperature on that day is close to the threshold temperature (Fig. 10). Thus, at lower elevations, which are mainly characterized by wetland/terrace, grassland and forest hillslopes, the precipitation was in the form of rainfall. The temperature and precipitation records show that the preceding days were dry and warm (Fig. 10), translating into comparatively elevated evaporation and, linked to that, relatively high soil moisture deficits. In addition, the deep root zone on the forest hillslopes provides considerable storage capacity in the soil before discharge is generated. At higher elevation, which is mainly characterized by bare soil/rock and grassland hillslopes, the precipitation was in solid state, subsequently stored as snowpack. When the temperature increased again in the following days, the snow melted gradually. However, due to the slow melt rates and the dry antecedent conditions, the snowmelt water was almost completely infiltrated into the groundwater and did not contribute to the storm flow, even when the temperature increased several days later (Fig. 10b–d). In summary, FLEX^T allowed the low and high elevation areas to reduce the storm flow for this specific event by different

mechanisms, resulting in a very limited response to the event, in close agreement with the observed response.

5.2   Translating topography information into hydrological models

It is intriguing to find that the landscape classification based on topography information (HAND, slope, elevation and aspect) closely reflects the patterns and shapes of the land cover map (Fig. 6a and b). In other words, it clearly illustrates that topography is an integrated indicator of energy and water availability and redistribution of natural vegetation cover's growing and evolving environment. Certain kinds of vegetation are naturally selected under specific topographical conditions (including elevation, aspect, HAND and slope). Elevation greatly influences the amount of precipitation and energy balance. HAND and slope are two important factors for the water retention and drainage. Aspect influences the energy balance and precipitation. Normally, the south-facing hillslopes receive more solar energy. Thus, the potential evaporation on the south-facing hillslopes is larger than on north-facing ones. Aspect influences the distribution of forest and grassland in arid/semi-arid regions. Topography does not only directly influence the groundwater level and the occurrence of SOF, but also controls the soil and vegetation cover in certain geologic and climatic condition, and consequently the dominant hydrological processes (Savenije, 2010). The presented modeling approach can therefore be seen as a step towards to making more efficient use of topographic information for use in conceptual hydrological models. The successfully linked topographic information, land cover classification and hydrological model structure, supports the hypothesis that topographic information can be used to distinguish landscape elements with different hydrological functions (Savenije, 2010; Wagener et al., 2007).

5.3   The value of soft data in hydrological modelling

Hydrological modelling should also be seen as an art (Savenije, 2009). To ensure that models better reflect our understanding of reality we should make use of our experi-

Title Page

Abstract | Introduction

Conclusions | References

Tables | Figures

◄◄ | ►►

◄ | ►

Back | Close

Full Screen / Esc

Printer-friendly Version

Interactive Discussion

Full Screen / Esc

Printer-friendly Version

Interactive Discussion

ence and creativity. In addition to available data, hydrologists often have extensive expert knowledge about specific study sites. However, this "soft" knowledge is regularly under-exploited in hydrological modeling (Seibert and McDonnell, 2002). Without the use of soft data and mere reliance on automatic calibration, hydrological models run the risk to perform well only as a result of mathematically optimal curve-fitting, which may be far from providing realistic process representations (Wagener, 2003; Gupta et al., 2008; Andréassian et al., 2012; Hrachowitz et al., 2013b). In general four types of soft data can be valuable for hydrological modelling. The first one is our explicit or inferred knowledge on the hydrological processes occurring in reality. In this study, streams in high elevation tributaries, characterized by a dominance of relatively erodible bare soil/rock exhibit relatively high levels of turbidity (Fig. 2e), thus indicating the importance of soil erosion, which in turn supports the existence of surface runoff in these locations. Another type of "soft" data is the expert knowledge on acceptable parameter ranges, such as the maximum storage of the unsaturated reservoir at the catchment scale (S_{Umax}), which is closely linked to root depth and soil structure and strongly depends on the ecosystem. The third kind of valuable "soft" data is the understanding of the relative magnitude of specific parameters in different landscapes (Gharari et al., 2013a), providing further constraints on model parameters, and eliminating unrealistic parameter combinations. For example, in this study it was argued that forest canopy, undergrowth and litter on forested hillslopes, can intercept more precipitation (I_{maxFH}) than grass dominated hillslopes (I_{maxGH}) (Table 6). Fourthly, simulation results can be constrained by "soft data", such as NDVI maps indicating inequalities between forest and grassland transpiration (Table 6). Making use of these four types of soft data, a topography driven model, FLEX^T, based our understanding of the hydrological processes in the Upper Heihe was developed and constrained. Although the use of these additional constraints resulted in slightly reduced performance of FLEX^T during calibration as compared to the lumped FLEX^L set-up, the successful nested sub-catchments validation demonstrated the value of soft data and clearly indicated that the efficient use of

soft data allows for a more realistic representation of catchment heterogeneity, leading to higher predictive power.

5.4 The role of forest in the Upper Heihe

Since forest is an important land cover in the Upper Heihe and many other catchments, the hydrological impact of forest is essential for understanding the catchment water cycle (Andréassian, 2004; Lyon et al., 2012), but also for an efficient implementation of water resource management policies. The role of forest on the catchment scale is subject of ongoing discussion in eco-hydrology (Sriwongsitanon and Taesombat, 2011; Moore and Wondzell, 2005). Various earlier studies found very diverse conclusions (Sahin and Hall, 1996; Moore and Wondzell, 2005; Bosch and Hewlett, 1982; Andréassian, 2004; Robinson et al., 1991). In this study, the FLEX^T model generated little runoff in forest hillslopes in the Upper Heihe, with most of the rainfall on the forest being intercepted and transpired. In addition, these results are supported by other studies in this catchment based on remote sensing information (Tian et al., 2013), statistical analysis (Wang et al., 2011), paired catchment analysis in this region (Qin et al., 2011; Huang et al., 2003), and the simulation of eco-hydrological model (Yu et al., 2009). On the other hand, field observations and experimental studies in the Upper Heihe (B. Ye, personal communication, 2012) also gave evidence of limited runoff from forest. This phenomenon is most likely linked to the climatic conditions in the Upper Heihe. Since the precipitation in this region reaches on average only 430 mm a^{-1}, with a maximum observed daily catchment average precipitation of below 45 mm d^{-1} (corrected by elevation), with ample storage available in the root zone, the forest hillslopes in the Upper Heihe remain largely below the moisture content necessary to establish connectivity conditions necessary to significantly contribute to storm flow.

6   Conclusions

We compared three model structures on the Upper Heihe in China: a lumped model (FLEX^L), a semi-distributed model with the same model structure (FLEX^D), and a conceptual model whose model structure is determined based on hypotheses of how topography influences hydrological processes (FLEX^T). FLEX^T performs slightly better than the two previous models in split-sample validation, but much better when validated in two nested sub-catchments. The increased performance of FLEX^T with respect to FLEX^L and FLEX^D in the nested sub-catchments, both in the flow duration curves and in some specific events, indicates that: (1) the topography-driven model structure, describing different dominant hydrological mechanisms in different landscapes, reflects the catchment heterogeneity in a more realistic way; (2) the natural land cover could be identified by topographic information to some extent, because the topography greatly influences the local energy and water budget; (3) the use of parameter and flux constraints guided by soft data, such as NDVI, reduced unrealistic compensation between fluxes and increased model transferability. In summary, making use of topography derived information to guide model development is a promising venue.

The simulated results of FLEX^T indicate a partitioning of water: 2/3 of the precipitation in this cold mountainous basin is evaporated back into atmosphere. Only 1/3 of the precipitation yields as runoff. The base flow contributes 36 % of the total runoff. The rest 64 % of the runoff comes from the surface/sub-surface fast runoff. The successful model simulation and nested sub-catchments transferability supports our perceptual model: most of the precipitation on the bare soil/rock in the summit of mountain feeds the groundwater and contributes to the base flow; the forest hillslopes produce limited runoff; grassland hillslopes and the wetland/terrace are the two main surface runoff generating regions; wetland/terrace has both strong evaporation and considerable surface runoff.

There are also limitations to this study. Firstly, there are uncertainties of input data, the model structure and the parameter sets; however we did not consider the uncer-

tainty in details due to the limited space. Secondly, there are several hypotheses of the proposed model structure that could not be tested individually for lack of available data. They will be further investigated during future research, using additional information.

References

Abbott, M. B. and Refsgaard, J. C.: Distributed Hydrological Modelling, Springer, Dordrecht, 1996. 12666

Andréassian, V.: Waters and forests: from historical controversy to scientific debate, J. Hydrol., 291, 1–27, 2004. 12691

Andréassian, V., Lerat, J., Le Moine, N., and Perrin, C.: Neighbors: nature's own hydrological models, J. Hydrol., 414–415, 49–58, 2012. 12690

Beven, K. and Germann, P.: Macropores and water flow in soils revisited, Water Resour. Res., 49, 3071–3092, 2013. 12666, 12670

Beven, K. J.: Rainfall-Runoff Modelling, Wiley-Blackwell, New Jersey, 2012. 12669

Beven, K. J. and Kirkby, M. J.: A physically based, variable contributing area model of basin hydrology, Hydrol. Sci. Bull., 24, 43–69, 1979. 12665

Bosch, J. M. and Hewlett, J. D.: A review of catchment experiments to determine the effect of vegetation changes on water yield and evapotranspiration, J. Hydrol., 55, 3–23, 1982. 12691

Chen, R. S., Kang, E., Yang, J. P., and Zhang, J. S.: Application of TOPMODEL to simulate runoff from Heihe mainstream mountainous basin, J. Desert Res., 23, 428–434, 2003. 12668

Dooge, J. C. I.: Bringing it all together, Hydrol. Earth Syst. Sci., 9, 3–14, doi:10.5194/hess-9-3-2005, 2005. 12665

Euser, T., Winsemius, H. C., Hrachowitz, M., Fenicia, F., Uhlenbrook, S., and Savenije, H. H. G.: A framework to assess the realism of model structures using hydrological signatures, Hydrol. Earth Syst. Sci., 17, 1893–1912, doi:10.5194/hess-17-1893-2013, 2013. 12667

Fenicia, F., Savenije, H. H. G., Matgen, P., and Pfister, L.: Is the groundwater reservoir linear? Learning from data in hydrological modelling, Hydrol. Earth Syst. Sci., 10, 139–150, doi:10.5194/hess-10-139-2006, 2006. 12680

Fenicia, F., Savenije, H. H. G., Matgen, P., and Pfister, L.: Understanding catchment behavior through stepwise model concept improvement, Water Resour. Res., 44, W01402, doi:10.1029/2006wr005563, 2008. 12666, 12667, 12672

Fenicia, F., Kavetski, D., and Savenije, H. H. G.: Elements of a flexible approach for conceptual hydrological modeling: 1. Motivation and theoretical development, Water Resour. Res., 47, W11510, doi:10.1029/2010wr010174, 2011. 12666, 12667, 12672

Gao, H., He, X., Ye, B., and Pu, J.: Modeling the runoff and glacier mass balance in a small watershed on the Central Tibetan Plateau, China, from 1955 to 2008, Hydrol. Process., 26, 1593–1603, doi:10.1002/hyp.8256, 2011. 12673

Gharari, S., Hrachowitz, M., Fenicia, F., and Savenije, H. H. G.: Hydrological landscape classification: investigating the performance of HAND based landscape classifications in a central European meso-scale catchment, Hydrol. Earth Syst. Sci., 15, 3275–3291, doi:10.5194/hess-15-3275-2011, 2011. 12666, 12677

Gharari, S., Hrachowitz, M., Fenicia, F., and Savenije, H.: Incorporating expert knowledge in a complex hydrological conceptual model: a FLEX-Topo case study for a central European meso-scale catchment, Hydrol. Earth Syst. Sci. Discuss., submitted, 2013a. 12690

Gharari, S., Hrachowitz, M., Fenicia, F., and Savenije, H. H. G.: An approach to identify time consistent model parameters: sub-period calibration, Hydrol. Earth Syst. Sci., 17, 149–161, doi:10.5194/hess-17-149-2013, 2013b. 12667

Grayson, R. and Blöschl, G.: Spatial Patterns in Catchment Hydrology: Observations and Modelling, Cambridge University Press, 2001. 12666

Gupta, H. V., Wagener, T., and Liu, Y.: Reconciling theory with observations: elements of a diagnostic approach to model evaluation, Hydrol. Process., 22, 3802–3813, 2008. 12667, 12690

Hamon, W.: Estimating potential evapotranspiration, J. Hydrol. Eng. Div.-ASCE, 87, 107–120, 1961. 12670

Hrachowitz, M., Savenije, H., Bogaard, T. A., Tetzlaff, D., and Soulsby, C.: What can flux tracking teach us about water age distribution patterns and their temporal dynamics?, Hydrol. Earth Syst. Sci., 17, 533–564, doi:10.5194/hess-17-533-2013, 2013a. 12673

Realism test of FLEX-Topo in the Upper Heihe

H. Gao et al.

Title Page

Abstract | Introduction

Conclusions | References

Tables | Figures

|◄ | ►|

◄ | ►

Back | Close

Full Screen / Esc

Printer-friendly Version

Interactive Discussion

Hrachowitz, M., Savenije, H. H. G., Blöschl, G., McDonnell, J. J., Sivapalan, M., Pomeroy, J. W., Arheimer, B., Blume, T., Clark, M. P., Ehret, U., Fenicia, F., Freer, J. E., Gelfan, A., Gupta, H. V., Hughes, D. A., Hut, R. W., Montanari, A., Pande, S., Tetzlaff, D., Troch, P. A., Uhlenbrook, S., Wagener, T., Winsemius, H. C., Woods, R. A., Zehe, E., and Cudennec, C.: A decade of Predictions in Ungauged Basins (PUB) – a review, Hydrolog. Sci. J., 58, 1198–1255, 2013b. 12666, 12667, 12682, 12690

Huang, M., Zhang, L., and Gallichand, J.: Runoff responses to afforestation in a watershed of the Loess Plateau, China, Hydrol. Process., 17, 2599–2609, 2003. 12691

Jia, Y., Ding, X., Qin, C., and Wang, H.: Distributed modeling of landsurface water and energy budgets in the inland Heihe river basin of China, Hydrol. Earth Syst. Sci., 13, 1849–1866, doi:10.5194/hess-13-1849-2009, 2009. 12668

Jin, X., Wan, L., and Hu, G.: Distribution characteristics of mountain vegetation and the influence factors in upstream of Heihe River Basin, J. Arid Land Resour. Env., 22, 140–144, 2008. 12677

Kang, E., Cheng, G., Lan, Y., Chen, R. S., and Zhang, J.: Application of a conceptual hydrological model in the runoff forecast of a mountainous watershed, Adv. Earth Sci., 17, 18–26, 2002. 12668

Kavetski, D. and Kuczera, G.: Model smoothing strategies to remove microscale discontinuities and spurious secondary optima in objective functions in hydrological calibration, Water Resour. Res., 43, W03411, doi:10.1029/2006wr005195, 2007. 12673

Khu, S.-T., Madsen, H., and di Pierro, F.: Incorporating multiple observations for distributed hydrologic model calibration: an approach using a multi-objective evolutionary algorithm and clustering, Adv. Water Resour., 31, 1387–1398, 2008. 12667

Klemeš, V.: Dilettantism in hydrology: transition or destiny?, Water Resour. Res., 22, 177S–188S, 1986. 12667, 12681

Klemeš, V.: The modelling of mountain hydrology: the ultimate challenge, IAHS report, London, 1990. 12671

Knudsen, J., Thomsen, A., and Refsgaard, J. C.: WATBAL a semi-distributed, physically based hydrological modelling system, Nord. Hydrol., 17, 347–362, 1986. 12665, 12666

Lamb, R. and Beven, K.: Using interactive recession curve analysis to specify a general catchment storage model, Hydrol. Earth Syst. Sci., 1, 101–113, doi:10.5194/hess-1-101-1997, 1997. 12680

Realism test of FLEX-Topo in the Upper Heihe

H. Gao et al.

Title Page

Abstract	Introduction
Conclusions	References
Tables	Figures

◄ ►|

◄ ►

| Back | Close |

Full Screen / Esc

Printer-friendly Version

Interactive Discussion

Li, Z., Xu, Z., and Li, Z.: Performance of WASMOD and SWAT on hydrological simulation in Yingluoxia watershed in northwest of China, Hydrol. Process., 25, 2001–2008, 2011. 12668

Lyon, S. W., Nathanson, M., Spans, A., Grabs, T., Laudon, H., Temnerud, J., Bishop, K. H., and Seibert, J.: Specific discharge variability in a boreal landscape, Water Resour. Res., 48, W08506, doi:10.1029/2011wr011073, 2012. 12691

Moore, R. D. and Wondzell, S. M.: Pysical hydrology and the effects of forest harvesting in the Pacific Northwest: a Review, JAWRA J. Am. Water Resour. As., 41, 763–784, 2005. 12691

Nash, J. E. and Sutcliffe, J. V.: River flow forecasting through conceptual models, Part 1 – A discussion of principles, J. Hydrol., 10, 282–290, 1970. 12679

Nobre, A., Cuartas, L., Hodnett, M., Rennó, C., Rodrigues, G., Silveira, A., Waterloo, M., and Saleska, S.: Height above the nearest drainage – a hydrologically relevant new terrain model, J. Hydrol., 404, 13–29, 2011. 12666, 12677

Pokhrel, P. and Gupta, H. V.: On the ability to infer spatial catchment variability using streamflow hydrographs, Water Resour. Res., 47, W08534, doi:10.1029/2010WR009873, 2011. 12667, 12681

Qin, J., Ding, Y., Ye, B., Zhou, Z., and Xie, Z.: Regulating effect of mountain landscapes on river runoff in Northwest China, J. Glaciol. Geocryol., 33, 397–404, 2011. 12691

Refsgaard, J. C. and Knudsen, J.: Operational validation and intercomparison of different types of hydrological models, Water Resour. Res., 32, 2189–2202, 1996. 12666

Rennó, C., Nobre, A., Cuartas, L., Soares, J., Hodnett, M., Tomasella, J., and Waterloo, M.: HAND, a new terrain descriptor using SRTM-DEM: mapping terra-firme rainforest environments in Amazonia, Remote Sens. Environ., 112, 3469–3481, 2008. 12666, 12677

Robinson, M., Gannon, B., and Schuch, M.: A comparison of the hydrology of moorland under natural conditions, agricultural use and forestry, Hydrolog. Sci. J., 36, 565–577, 1991. 12691

Sahin, V. and Hall, M. J.: The effects of afforestation and deforestation on water yields, J. Hydrol., 178, 293–309, 1996. 12691

Savenije, H. H. G.: Determination of evaporation from a catchment water balance at a monthly time scale, Hydrol. Earth Syst. Sci., 1, 93–100, doi:10.5194/hess-1-93-1997, 1997. 12674

Savenije, H. H. G.: HESS Opinions "The art of hydrology"*, Hydrol. Earth Syst. Sci., 13, 157–161, doi:10.5194/hess-13-157-2009, 2009. 12689

Savenije, H. H. G.: HESS Opinions "Topography driven conceptual modelling (FLEX-Topo)", Hydrol. Earth Syst. Sci., 14, 2681–2692, doi:10.5194/hess-14-2681-2010, 2010. 12665, 12666, 12667, 12670, 12689

Title Page

Abstract | Introduction

Conclusions | References

Tables | Figures

|◄ | ►|

◄ | ►

Back | Close

Full Screen / Esc

Printer-friendly Version

Interactive Discussion

Scherrer, S. and Naef, F.: A decision scheme to indicate dominant hydrological flow processes on temperate grassland, Hydrol. Process., 17, 391–401, 2003. 12666

Seibert, J.: Estimation of parameter uncertainty in the HBV model, Nord. Hydrol., 28, 247–262, 1997. 12673

5 Seibert, J. and McDonnell, J. J.: On the dialog between experimentalist and modeler in catchment hydrology: use of soft data for multicriteria model calibration, Water Resour. Res., 38, 1241, doi:10.1029/2001wr000978, 2002. 12667, 12690

Sivapalan, M.: The secret to "doing better hydrological science": change the question!, Hydrol. Process., 23, 1391–1396, 2009. 12665

10 Sivapalan, M., Takeuchi, K., Franks, S. W., Gupta, V. K., Karambiri, H., Lakshmi, V., Liang, X., McDonnell, J. J., Mendiondo, E. M., O'Connell, P. E., Oki, T., Pomeroy, J. W., Schertzer, D., Uhlenbrook, S., and Zehe, E.: IAHS decade on Predictions in Ungauged Basins (PUB), 2003–2012: shaping an exciting future for the hydrological sciences, Hydrolog. Sci. J., 48, 857–880, 2003. 12682

15 Spence, C. and Woo, M.-K.: Hydrology of subarctic Canadian shield: soil-filled valleys, J. Hydrol., 279, 151–166, 2003. 12665

Sriwongsitanon, N. and Taesombat, W.: Effects of land cover on runoff coefficient, J. Hydrol., 410, 226–238, 2011. 12691

Tetzlaff, D., Soulsby, C., Buttle, J., Capell, R., Carey, S. K., Laudon, H., McDonnell, J.,
20 McGuire, K., Seibert, J., and Shanley, J.: Catchments on the cusp? Structural and functional change in northern ecohydrology, Hydrol. Process., 27, 766–774, 2013. 12669

Tian, F., Qiu, G., Yang, Y., Lü, Y., and Xiong, Y.: Estimation of evapotranspiration and its partition based on an extended three-temperature model and MODIS products, J. Hydrol., 498, 210–220, 2013. 12691

25 Tromp-van Meerveld, H. J. and McDonnell, J. J.: Threshold relations in subsurface stormflow: 2. The fill and spill hypothesis, Water Resour. Res., 42, W02411, doi:10.1029/2004wr003800, 2006. 12665

Uhlenbrook, S. and Leibundgut, C.: Process-oriented catchment modelling and multiple-response validation, Hydrol. Process., 16, 423–440, 2002. 12667

30 Uhlenbrook, S., Roser, S., and Tilch, N.: Hydrological process representation at the meso-scale: the potential of a distributed, conceptual catchment model, J. Hydrol., 291, 278–296, 2004. 12665, 12673

Title Page

Abstract | Introduction

Conclusions | References

Tables | Figures

|◀ | ▶|

◀ | ▶

Back | Close

Full Screen / Esc

Printer-friendly Version

Interactive Discussion

Vrugt, J. A., Gupta, H. V., Bastidas, L. A., Bouten, W., and Sorooshian, S.: Effective and efficient algorithm for multiobjective optimization of hydrologic models, Water Resour. Res., 39, 1214, doi:10.1029/2002wr001746, 2003. 12680

Wagener, T.: Evaluation of catchment models, Hydrol. Process., 17, 3375–3378, 2003. 12690

Wagener, T., Sivapalan, M., Troch, P., and Woods, R.: Catchment classification and hydrologic similarity, Geogr. Compass, 1, 901–931, 2007. 12689

Wang, J., Li, H., and Hao, X.: Responses of snowmelt runoff to climatic change in an inland river basin, Northwestern China, over the past 50 years, Hydrol. Earth Syst. Sci., 14, 1979–1987, doi:10.5194/hess-14-1979-2010, 2010. 12668

Wang, N.: Isotope hydrology in Heihe, Chinese Sci. Bull., 54, 2148–2152, 2009. 12671

Wang, Y., Yu, P., Feger, K., Wei, X., Sun, G., Bonell, M., Xiong, W., Zhang, S., and Xu, L.: Annual runoff and evapotranspiration of forestlands and non-forestlands in selected basins of the Loess Plateau of China, Ecohydrology, 4, 277–287, 2011. 12691

Western, A. W., Grayson, R. B., Blöschl, G., Willgoose, G. R., and McMahon, T. A.: Observed spatial organization of soil moisture and its relation to terrain indices, Water Resour. Res., 35, 797–810, 1999. 12665

Xia, J., Wang, G. S., Lv, A. F., and Tan, G.: A research on distributed time variant gain modeling, Acta Geographica Sinica, 58, 789–796, 2003. 12668

Yu, P., Krysanova, V., Wang, Y., Xiong, W., Mo, F., Shi, Z., Liu, H., Vetter, T., and Huang, S.: Quantitative estimate of water yield reduction caused by forestation in a water-limited area in northwest China, Geophys. Res. Lett., 36, L02406, doi:10.1029/2008gl036744, 2009. 12691

Zang, C. F., Liu, J., van der Velde, M., and Kraxner, F.: Assessment of spatial and temporal patterns of green and blue water flows under natural conditions in inland river basins in Northwest China, Hydrol. Earth Syst. Sci., 16, 2859–2870, doi:10.5194/hess-16-2859-2012, 2012. 12668

Zhao, R.-J.: The Xinanjiang model applied in China, J. Hydrol., 135, 371–381, 1992. 12665, 12674

Zhou, J., Li, X., Wang, G., Hu, H. C., and Chao, Z. H.: An improved precipitation-runoff model based on MMS and its application in the upstream basin of the Heihe River, J. Nat. Res., 23, 724–736, 2008. 12668

Title Page

Abstract | Introduction

Conclusions | References

Tables | Figures

|◄ | ►|

◄ | ►

Back | Close

Full Screen / Esc

Printer-friendly Version

Interactive Discussion

Table 1. Summary of four the meteorological stations in and close to the Upper Heihe.

Station	Elevation (m)	Latitude (°)	Longitude (°)	Thiessen area ratio (%)	Precipitation $(mm\,a^{-1})$	Annual average daily temperature (°C)	Potential Evaporation $(mm\,a^{-1})$
Zhangye	1484	38.93	100.43	4	131	7.1	804
Yeniugou	3320	38.42	99.58	43	413	−3.2	392
Qilian	2788	38.18	100.25	40	394	0.8	513
Tuole	3368	38.80	98.42	13	293	−3.0	421

Table 2. Catchment characteristics of the entire Upper Heihe and two sub-catchments, Qilian and Zhamashike.

	Latitude (°)	Longitude (°)	Average Elevation (m)	Area (km^2)	Discharge (mm a^{-1})
Yingluoxia (Upper Heihe)	38.80	100.17	3661	10 009	145
Qilian (East tributary)	38.19	100.24	3535	2924	142
Zhamashike (West tributary)	38.23	99.98	3990	5526	124

Table 3. Proportion of different landscape units in the study catchments.

	Wetland/Terrace (%)	Grassland Hillslope (%)	Forest Hillslope (%)	Bare soil/rock (%)
Heihe	36	31	17	16
Qilian	33	28	25	14
Zhamashike	46	33	6	15

Title Page

Abstract | Introduction

Conclusions | References

Tables | Figures

◄◄ | ►►

◄ | ►

Back | Close

Full Screen / Esc

Printer-friendly Version

Interactive Discussion

Table 4. Uniform prior parameter distributions of the FLEX^L and FLEX^D models.

Parameter	Range
F_{DD} (mm (d °C)$^{-1}$)	(1, 8)
T_t (°C)	(−2.5, 2.5)
I_{max} (mm d^{-1})	(0.1, 5)
S_{Umax} (mm)	(50, 1000)
β (−)	(0.1, 5)
D (−)	(0, 1)
K_s (d)	90
S_{fmax} (mm)	(10, 200)
K_{ff} (d)	(1, 5)
K_f (d)	(1, 20)
T_{lag} (d)	(0, 5)
T_{lagT} (d)	(0, 5)
T_{lagY} (d)	(0, 5)
T_{lagQ} (d)	(0, 5)

Discussion Paper | Discussion Paper | Discussion Paper | Discussion Paper

HESSD

10, 12663–12716, 2013

Realism test of FLEX-Topo in the Upper Heihe

H. Gao et al.

Title Page

Abstract | Introduction

Conclusions | References

Tables | Figures

|◀ | ▶|

◀ | ▶

Back | Close

Full Screen / Esc

Printer-friendly Version

Interactive Discussion

Table 5. Uniform prior parameter distributions of the FLEX^T model.

Parameters in all 3 models	Range	Parameters for bare soil/rock	Range	Parameter for forest hillslope	Range
F_{DD} (mm (d°C)$^{-1}$)	(1, 8)	S_{UmaxB} (mm)	(5, 500)	I_{maxFH} (mm d^{-1})	(1, 10)
T_t (°C)	(−2.5, 2.5)	P_{maxB} (mm d^{-1})	(0.1, 10)	S_{UmaxFH} (mm)	(100, 1000)
P_t (mm d^{-1})	(5, 35)	D_B (−)	(0, 1)	β_{FH} (−)	(0.1, 5)
K_f (d)	(1, 20)	K_{ff} (d)	(2, 50)		
K_s (d)	90				
D (-)	(0, 1)				
T_{lagT} (d)	(0, 5)				
T_{lagY} (d)	(0, 5)				
T_{lagQ} (d)	(0, 5)				
Parameter for grass hillslope	Range	Parameter for wetland	Range		
I_{maxGH} (mm d^{-1})	(0, 10)	I_{maxW} (mm d^{-1})	(0.1, 10)		
S_{UmaxGH} (mm)	(50, 1000)	S_{UmaxW} (mm)	(5, 1000)		
β_{GH} (−)	(0.1, 5)	β_W (−)	(0.1, 5)		
		C_R (mm d^{-1})	(0.01, 2)		
		K_r (d)	(1, 9)		

Table 6. The soft data to constrain the automatic calibration.

Soft parameter constraint based on perceptual realism	Soft performance constraint based on NDVI map
$I_{maxFH} > I_{maxGH}$	$E_{iFH} + E_{aFH} > E_{iGH} + E_{aGH}$
$I_{maxFH} > I_{maxW}$	$E_{iW} + E_{aW} > E_{iGH} + E_{aGH}$
$S_{UmaxFH} > S_{UmaxGH} > S_{UmaxW}$	$E_{iGH} + E_{aGH} > E_{aB}$
$S_{UmaxFH} > S_{UmaxGH} > S_{UmaxB}$	$E_{aFH} > E_{aGH}$
$K_s > K_f > K_{ff}$	
$K_s > K_f > K_r$	

Table 7. The averaged results of all the points on the Pareto front of three objective functions of the three models FLEX^L, FLEX^D and FLEX^T in calibration, split-sample and nested sub-catchments validation.

	Calibration			Split-sample validation			Zhamashike validation			Qilian validation		
	I_{NS}	I_{NSF}	I_{NSL}	I_{NS}	I_{NSF}	I_{NSL}	I_{NS}	I_{NSF}	I_{NSL}	I_{NS}	I_{NSF}	I_{NSL}
FLEX^L	0.82	0.99	0.87	0.79	0.95	0.78	0.54	0.79	0.56	0.56	0.87	0.59
FLEX^D	0.81	0.99	0.84	0.74	0.94	0.76	0.56	0.83	0.6	0.53	0.84	0.58
FLEX^T	0.80	0.98	0.84	0.78	0.95	0.82	0.65	0.92	0.74	0.71	0.96	0.75
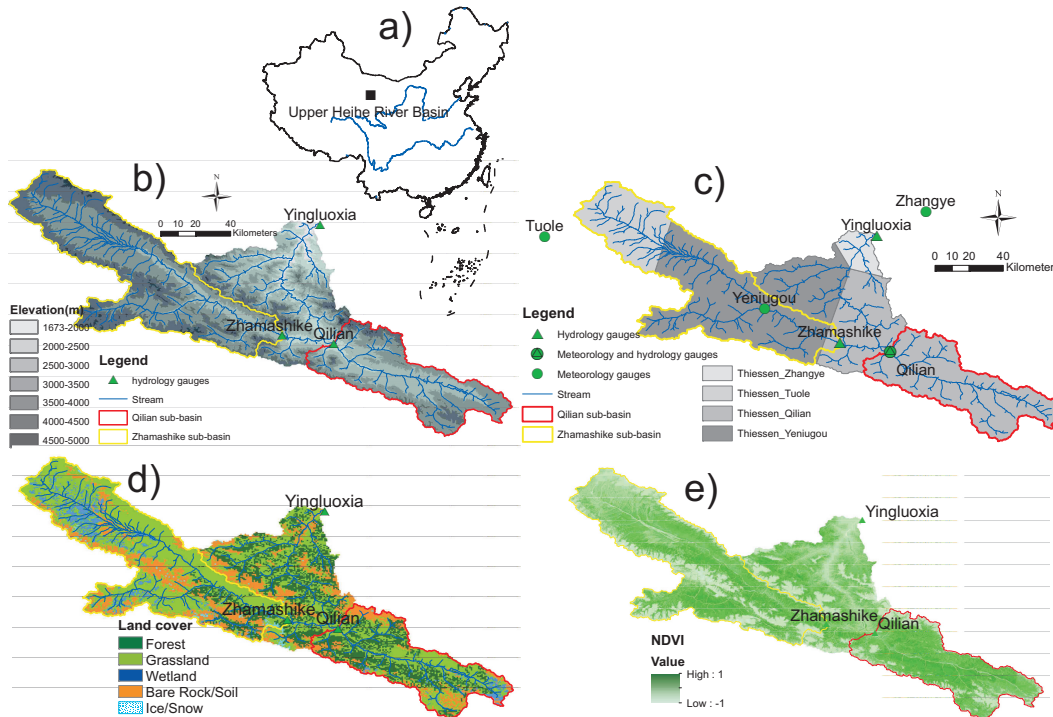
Fig. 1. (a) location of the Upper Heihe in China; **(b)** DEM of the Upper Heihe with its runoff gauging stations, meteorological stations, streams and the outline of two sub-catchments; **(c)** meteorological stations and associated Thiessen polygons, the different grayscale indicates different long term annual average precipitation (the darker the more precipitation: Zhangye is 131 $(mm\,a^{-1})$; Tuole is 293 $(mm\,a^{-1})$; Qilian is 394 $(mm\,a^{-1})$; Yeniugou is 413 $(mm\,a^{-1})$); **(d)** land cover map of the Upper Heihe; **(e)** averaged NDVI map in the summer of 2002.

Title Page

Abstract · Introduction

Conclusions · References

Tables · Figures

|◄ · ►|

◄ · ►

Back · Close

Full Screen / Esc

Printer-friendly Version

Interactive Discussion
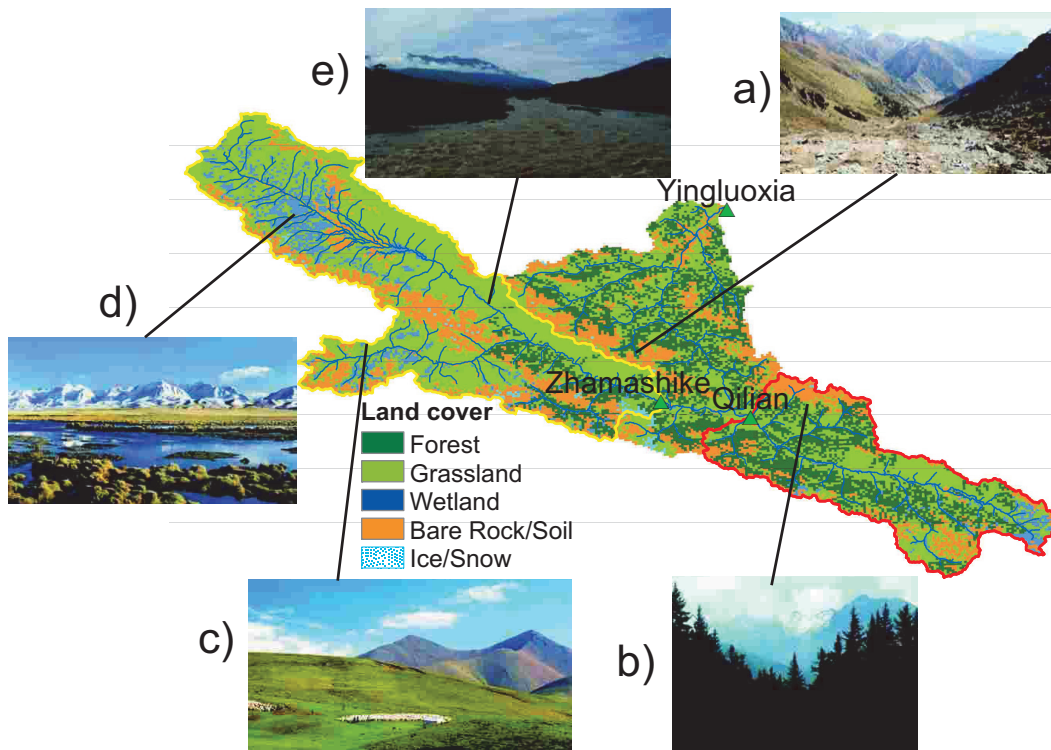
Fig. 2. Characteristic landscapes in different locations in the Upper Heihe.

Fig. 3. The lumped model structure FLEX^L.
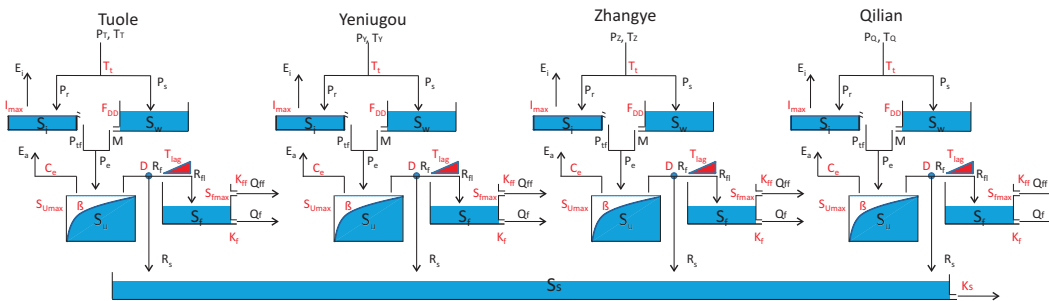
Fig. 4. The semi-distributed model structure FLEX^D. (Note that, for better readability, only the four parallel model structures representing the four Thiessen polygons in the study area are shown here.)
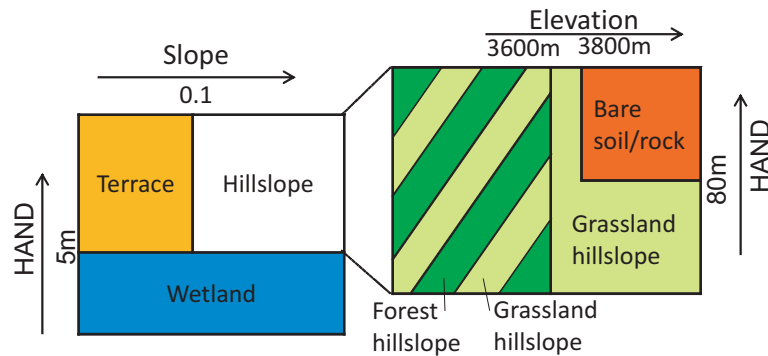
Fig. 5. Summary of the landscape classification criteria.

Title Page

Abstract | Introduction

Conclusions | References

Tables | Figures

|◀ | ▶|

◀ | ▶

Back | Close

Full Screen / Esc

Printer-friendly Version

Interactive Discussion
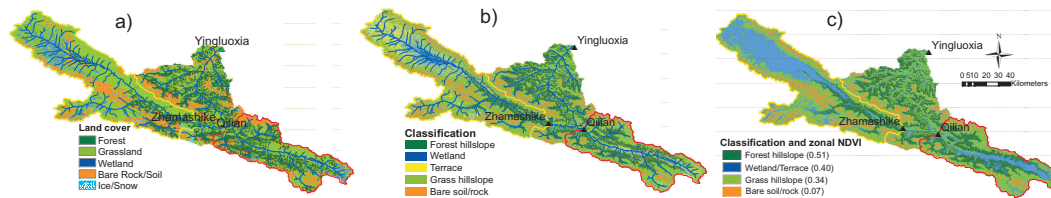
Fig. 6. Comparison of land cover **(a)** and landscape classification maps **(b, c)**, and the NDVI in each land cover **(c)**.
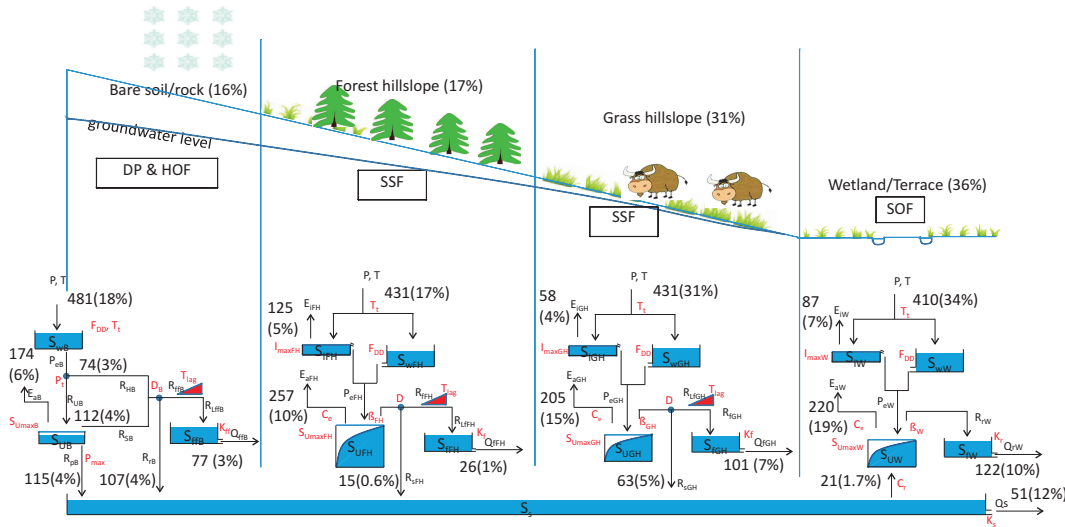
Fig. 7. Perceptual model and parallel model structures of FLEX^T for the Upper Heihe, and the simulated fluxes. The unit of all the fluxes is given in $\mathrm{mm\,a^{-1}}$ for each landscape element, except for the groundwater flow which is the flux over the entire catchment. The percentages in brackets indicate the rainfall (100 %) partitioning within the catchment.

Title Page

Abstract | Introduction

Conclusions | References

Tables | Figures

◄◄ | ►►

◄ | ►

Back | Close

Full Screen / Esc

Printer-friendly Version

Interactive Discussion
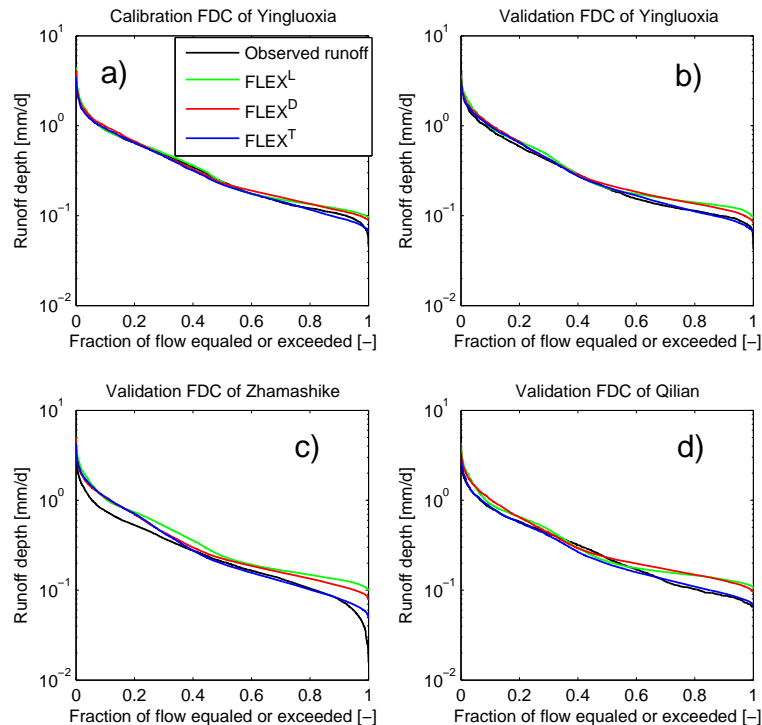
Fig. 8. Calibration **(a)** and validation results for the flow duration curve of three models for the total catchment **(b)** and two nested catchments **(c, d)**. The curves make use of the average value of the parameter sets on the Pareto-optimal front.
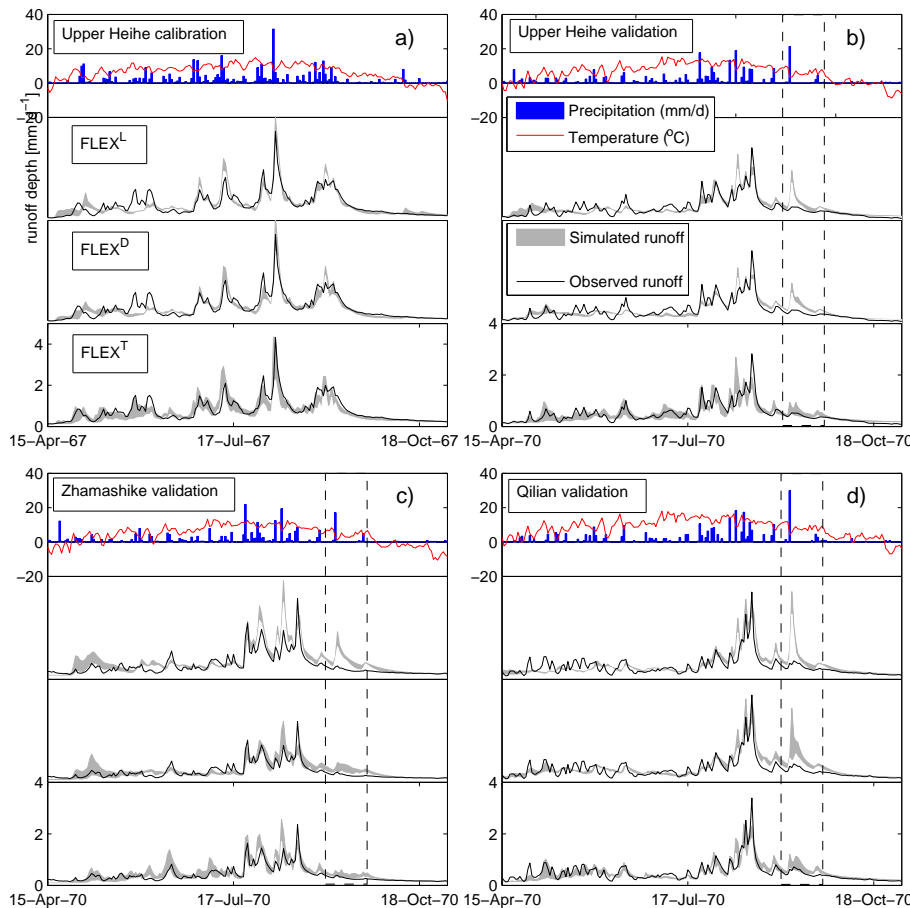
Fig. 9. Comparison between observed and simulated hydrographs (from all Pareto-optimal models) of three model structures, in the calibration period **(a)**, split-sample validation **(b)** and nested sub-catchments validation **(c, d)**. Precipitation and temperature are also shown.
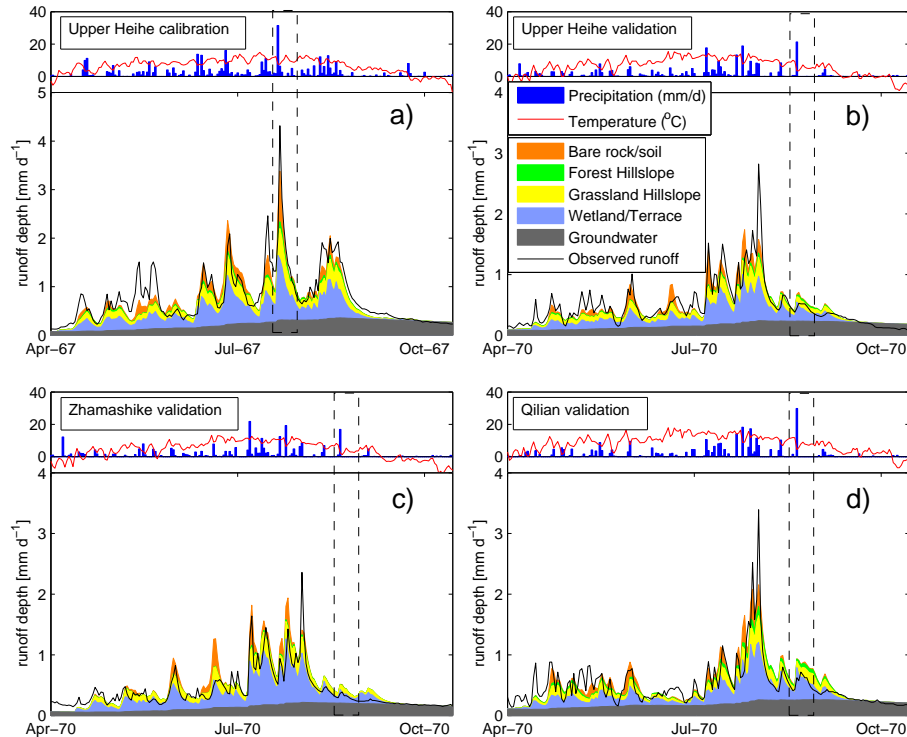
Fig. 10. The hydrograph components of the calibration **(a)**, split-sample validation **(b)** and nested sub-catchments validation **(c, d)**, of the FLEX^T model (using the average value of the parameter sets on the Pareto-optimal front).
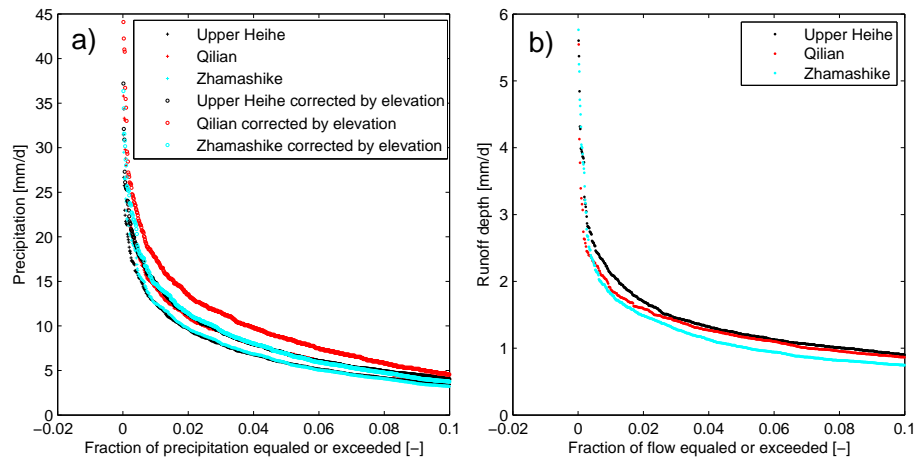
Fig. 11. The comparison of three observed precipitation duration curves **(a)** and flow duration curves **(b)**.